Journal of Contaminant Hydrology 182 (2015) 1–15

Contents lists available at ScienceDirect

Journal of Contaminant Hydrology

journal homepage: www.elsevier.com/locate/jconhyd

Upscaling transport of a reacting solute through a peridocially converging–diverging channel at pre-asymptotic times

Nicole L. Sund [a], Diogo Bolster [a,*], Clint Dawson [b]

[a] Environmental Fluid Dynamics Laboratories, Department of Civil and Environmental Engineering and Earth Sciences, University of Notre Dame, IN, USA
[b] The Institute for Computational Engineering and Sciences, The University of Texas at Austin, Austin, TX 78712, USA

ARTICLE INFO

Article history:
Received 24 May 2015
Received in revised form 6 August 2015
Accepted 9 August 2015
Available online 15 August 2015

Keywords:
Reactive transport
Upscaling
Spatial Markov model

ABSTRACT

In this study we extend the Spatial Markov model, which has been successfully used to upscale conservative transport across a diverse range of porous media flows, to test if it can accurately upscale reactive transport, defined by a spatially heterogeneous first order degradation rate. We test the model in a well known highly simplified geometry, commonly considered as an idealized pore or fracture structure, a periodic channel with wavy boundaries. The edges of the flow domain have a layer through which there is no flow, but in which diffusion of a solute still occurs. Reactions are confined to this region. We demonstrate that the Spatial Markov model, an upscaled random walk model that enforces correlation between successive jumps, can reproduce breakthrough curves measured from microscale simulations that explicitly resolve all pertinent processes. We also demonstrate that a similar random walk model that does not enforce successive correlations is unable to reproduce all features of the measured breakthrough curves.

1. Introduction

Modeling the transport of chemical species through a porous medium can involve many complex biogeochemical processes that can be distributed unevenly in space (Dentz et al., 2011). At the same time the geometry of the flow domain gives rise to heterogeneous flow fields with fast and slow regions of potentially converging and diverging flow. Even in the case of conservative transport, this broad range of scales can complicate the development of effective models, which aim to describe transport without explicitly resolving all small scale features (Brenner, 1980; Plumb and Whitaker, 1988; Hornung, 1997). Add to this an additional range of timescales for reactive transport and the challenge can be even greater (Dentz et al., 2011).

In the case of conservative transport, the development of effective models for transport can in many ways be dated back to the seminal work of GI Taylor and Aris (Taylor, 1953; Aris, 1956), who demonstrated that after asymptotic times, transport of a solute through a cylindrical tube under laminar flow conditions, can be effectively described by a one-dimensional advection dispersion equation, with an enhanced dispersion coefficient. This enhanced dispersion coefficient represents the enhanced spreading that occurs due to the interplay of the heterogeneous (shear) velocity field and transverse diffusion. The arguments developed hold for any pure shear flow with the magnitude of the dispersion coefficient depending on the structure of that flow and the magnitude of the transverse diffusion coefficient. Building on these ideas a rich suite of modeling approaches, including the method of moments (Brenner, 1980), volume averaging (Plumb and Whitaker, 1988) and homogenization (Hornung, 1997), generalized Taylor's ideas to more complex geometries and the use of effective dispersion coefficients is widespread across disciplines.

Many of these ideas have been further generalized to the case of reactive transport. For example, Shapiro and Brenner (1988), using the method of moments, developed an effective upscaled equation for macroscopic transport that takes the

* Corresponding author.
E-mail address: dbolster@nd.edu (D. Bolster).

http://dx.doi.org/10.1016/j.jconhyd.2015.08.003
0169-7722/

form of an advection dispersion reaction equation, but with an effective dispersion coefficient, an effective velocity and an effective reaction rate, each of which depend on the specific makeup of microscale flow and reaction characteristics. Note that the effective velocity and dispersion coefficients can vary significantly from their conservative counterparts. Dykaar and Kitanidis (1996) used Shapiro and Brenner's method of moments approach, to calculate the effective dispersion, velocity and reaction rates for a highly idealized geometry: a vertically bounded, horizontally periodic channel with sinusoidally varying boundaries and a reactive region of uniform thickness that separates the flowing fluid and solid boundary. In particular, they showed that for high Damkohler number, the effective velocity and effective reaction rate vary greatly with Peclet number.

While incredibly powerful, these approaches in their original form, are strictly speaking only valid at asymptotic times. Throughout this document, by asymptotic times we mean times greater than the Taylor dispersion timescale, which is typically given by $\tau_D = L^2/D$, where L is a characteristic length scale and D the diffusion coefficient. That is, the equation is not valid at pre-asymptotic times, or times smaller than this. Depending on one's interests this may be reasonable or not, in which case a pre-asymptotic model may be desirable. Many of the aforementioned approaches can be generalized further to achieve this (Lunati et al., 2002; Wood et al., 2003; Richmond et al., 2013). However some recent studies have demonstrated that some of the assumptions required to close these theories for reactive transport can be quite restrictive and confine their regime of validity (Battiato et al., 2009; Battiato and Tartakovsky, 2011).

Here we propose an alternative modeling strategy, based on the Spatial Markov model (Le Borgne et al., 2008a), which to date has shown great promise in upscaling conservative transport all the way from pre-asymptotic to asymptotic times across a breadth of flows relevant to porous media. This includes transport through highly heterogeneous porous media (Le Borgne et al., 2008a, 2008b), fracture networks (Kang et al., 2011), idealized two-dimensional pore networks (Le Borgne et al., 2011; De Anna et al., 2013; Bolster et al., 2014), real three-dimensional pore systems (Kang et al., 2014), unsteady flows through porous media (Sund et al., in press), and most recently a field scale application to a fractured aquifer (Kang et al., 2015). The model is a subclass of the more general family of continuous time random walk (CTRW) models (Berkowitz et al., 2006) (indeed the Spatial Markov model has also gone by the name correlated CTRW). The idea behind the model is to discretize the concentration field, like any random walk model, into a large number of particles. These particles then transition through space and time following probabilistic rules that macroscopically replicate the small scale dynamics. Often random walks treat successive jumps as uncorrelated, independent and identically distributed. What distinguishes the Spatial Markov model is that successive jumps are correlated, a requirement we argue is needed to replicate the microscale behaviors, particularly when advective effects are dominant relative to diffusive ones (Bolster et al., 2014). It should be noted that the idea of a correlated random walk is in itself not a novel idea. Indeed works relating to correlated random walks date back almost a century; (e.g. Taylor, 1922), where GI Taylor showed a formal link between a form of correlated (*persistent*) random walk and the Telegraphers equation. Later works further explored these ideas (Goldstein, 1951; Gillis, 1955) and several more general reviews discuss correlated random walks (e.g. Haus and Kehr, 1987; Weiss and Rubin, 1983). The novelty of the Spatial Markov model lies in treating temporal jumps as random and encoding one step correlations in a numerically efficient manner via a measured transition matrix (Le Borgne et al., 2008a).

To date this modeling framework has only been applied to the case of conservative transport and here we test its ability to predict reactive transport associated with a thin reactive region with a first order degradation rate, by applying it to the simple case proposed by Dykaar and Kitanidis (1996), discussed above. While incredibly simple, this geometry appears to capture a rich array of dynamics, representative of important features of flow and transport in porous media. Multiple studies, using this or very similar geometries have been conducted to explore the effects of inertia on upscaling flow (Chaudhary et al., 2011, 2013) and transport (Bouquain et al., 2012; Bolster et al., 2014), studying the role of geometry on asymptotic (Cardenas, 2009; Bolster et al., 2009) and pre-asymptotic transport (Cardenas, 2008; Le Borgne et al., 2012), and studying the effects of turbulence on dispersion (Richmond et al., 2013) to name a few. Thus, while we recognize that the model geometry is very simple, we consider this simplicity as a strength and given its historical successes, we believe it is an ideal initial testbed for application of a Spatial Markov model to upscaling of reactive transport.

2. Model system

2.1. Geometry

The geometry we consider in this study is depicted in Fig. 1; the boundaries of the flowing fluid system are described by

$$h(x) = \overline{h} + h' \sin\left(\frac{2\pi x}{L} - \frac{\pi}{2}\right), \tag{1}$$

where x is the horizontal coordinate, $h(x)$ is the half-aperture, $\overline{h}$ is the mean half-aperture, h' is the amplitude fluctuation of the half-aperture and L is the length of a single cell. A reactive layer of uniform thickness b lies between the fluid phase and the solid matrix. In this study, to be consistent with Dykaar and Kitanidis (1996), we restrict ourselves to the case where $\overline{h} = L/4$, $h' = 0.8\overline{h}$ and $b = 0.4\overline{h}$.

2.2. Flow field

Fig. 1 also depicts the streamlines for the flow, which are calculated using a semi-analytical solution developed by Kitanidis and Dykaar (1997); and Dykaar and Kitanidis (1996). The solution assumes Stokes flow, that is Reynolds number much less than one, generally accepted as a good approximation for flow through porous media. For Stokes flow of an incompressible fluid, the velocity field $\mathbf{u}$ follows,

$$\frac{1}{\rho}\nabla P = \nu\nabla^2\mathbf{u} \quad \nabla\cdot\mathbf{u} = 0, \tag{2}$$

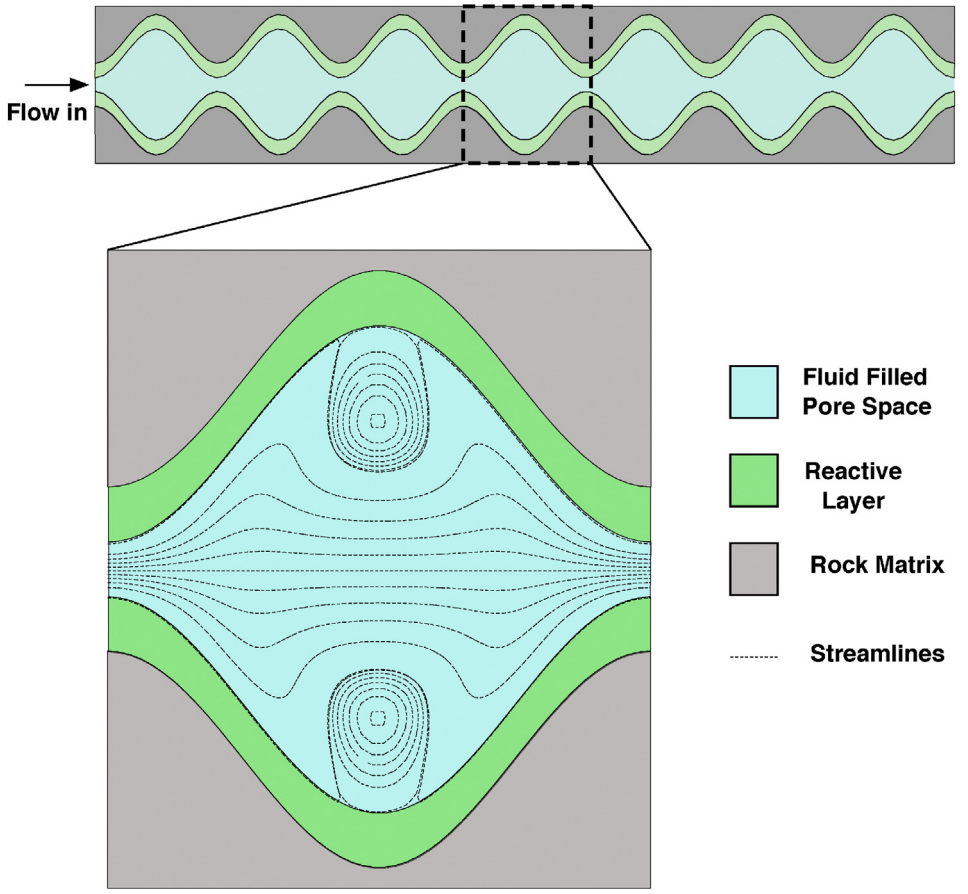

Fig. 1. Schematic of flow domain (top) and the unit cell 'pore' (bottom) for flow and transport modeling in this work. Streamlines for the flow are calculated using the semi-analytical solution for Stokes flow developed by Kitanidis and Dykaar (1997).

where P is the pressure, ρ is the density, and v is the kinematic viscosity of the fluid. These equations can be combined and written in terms of a stream function ψ, the governing equation of which is the biharmonic equation $\nabla^4\psi = 0$. The solution to this equation is built using a perturbation analysis assuming small $\epsilon = 2\bar{h}/L$, which here equals 0.5. While this choice of ϵ is not extremely small, it is sufficiently so, as the lowest order of the discarded terms in the expansion is ϵ^6. Also it is consistent with the original work using this geometry by Dykaar and Kitanidis (1996), who later showed that it compares favorably with the flow calculated by numerical means (Cao and Kitanidis, 1998). Details of this solution are available from multiple sources including Kitanidis and Dykaar (1997); Dykaar and Kitanidis (1996); Bolster et al. (2009) and so are not presented explicitly here.

2.3. Simulation of transport at the microscale

We consider reactive solute transport as governed by the advection diffusion reaction equation

$$\frac{\partial C(\mathbf{x},t)}{\partial t} + \mathbf{u}(\mathbf{x})\cdot\nabla C(\mathbf{x},t) = D\nabla^2 C(\mathbf{x},t) - \gamma(\mathbf{x})C(\mathbf{x},t), \tag{3}$$

where $C(\mathbf{x}, t)$ is the concentration of the solute and D is the molecular diffusion coefficient, taken to be constant in the fluid and reactive layer and zero in the solid matrix. $\gamma(\mathbf{x})$ is the reaction rate, which is taken as a constant α in the reactive layer and zero elsewhere. We consider here a first order kinetic reaction, which can be seen as a small concentration approximation to a Monod type relationship (Pavlostathis and Giraldo-Gomez, 1991; Semprini and McCarty, 1992). Boundary conditions are no-flux at the reactive layer solid matrix interface. In all cases we consider a pulse initial condition, flux weighted along the pore throat ($C(\mathbf{x}, t = 0) \propto \mathbf{u}(\mathbf{x})\delta(x)$).

To solve this system we implement a numerical Lagrangian particle based random walk method (Risken, 1984), where the solute plume is discretized into a finite number of N particles. For a given time step Δt each particle i is moved according to the Langevin equation

$$\begin{aligned} x_i(t+\Delta t) &= x_i(t) + u_i\Delta t + \xi_i\sqrt{2D\Delta t} \\ y_i(t+\Delta t) &= y_i(t) + v_i\Delta t + \eta_i\sqrt{2D\Delta t} \end{aligned} \quad i = 1,\ldots,N, \tag{4}$$

where x_i and y_i are the horizontal and vertical position of particle i respectively and ξ and η are independently distributed Gaussian variables with zero mean and unit variance. The solid boundaries in the domain are modeled as elastic reflection

boundaries, that is, if $\mathbf{x}_i(t+\Delta t)$ lies across a solid boundary, then its reflected position is

$$\mathbf{x}_i^r(t+\Delta t) = 2[\mathbf{x}_i(t) + \mathrm{proj}_\Gamma(\mathbf{x}_i(t+\Delta t) - \mathbf{x}_i(t))] - \mathbf{x}_i(t+\Delta t) \quad (5)$$

where proj_Γ is the projection onto the solid boundary Γ. The reaction term is implemented probabilistically, as in Kinzelbach (1988), by determining the probability P that a particle undergoes a reaction during a given time step, where

$$P = 1 - e^{-\gamma(\mathbf{x})\Delta t}, \quad (6)$$

where $P = 0$ if the particle is in the flowing fluid and $P = 1 - e^{-\alpha\Delta t}$ if the particle is in the reactive layer. This number P is then compared to a random number U, drawn from a standard uniform distribution. If $U \geq P$ no reaction occurs and if $U<P$ the reaction occurs and the particle is removed from the system.

We choose to use the Lagrangian random walk method for various reasons, including the following: (i) it allows for easy and effective calculation of breakthrough curves (BTCs) and (ii) given the periodic nature of the flow domain it makes it possible to consider transport through a very large number of unit cells without requiring a prohibitively large numerical mesh as only the particle's position relative to the unit periodic cell is required to calculate its velocity. For all simulations presented here one million particles were used and time steps of $\Delta t = 10^{-3}$ were chosen. The time step was chosen based on a convergence test (results with a time step 10 times smaller are virtually indistinguishable in terms of measured BTCs, discussed below) and is consistent with choices from previous studies on similar domains (Bolster et al., 2009).

2.4. Dimensionless numbers

The above system can be characterized by several dimensionless numbers given by

$$Re = \frac{2\bar{h}\bar{u}}{\nu} \qquad Sc = \frac{\nu}{D} \qquad Pe = \frac{2\bar{h}\bar{u}}{D} \qquad Da = \frac{4\bar{h}^2\alpha}{D} \quad (7)$$

where Re is the Reynolds number, Sc the Schmidt number, Pe the Peclet number and Da the Damkohler number. $\bar{u}$ is the average velocity in the fluid domain. Dykaar and Kitanidis (1996) provide typical ranges for these numbers as $10^{-4} < Re < 10^{-1}$, $500 < Sc < 2500$, $0.1 < Pe < 10^3$, $0 < Da < 10^4$. Since $Re \ll 1$ we are in the typical Stokes flow regime where the semi-analytical solution of the flow, given by Kitanidis and Dykaar (1997) based on Stokes flow, holds. A Schmidt number of $O(1000)$ indicates that while advective effects may be unimportant with regard to flow, they can still be important with regard to transport as diffusion coefficients for solutes are typically several orders of magnitude less than diffusion of fluid momentum (viscosity). The range of Damkohler numbers suggests that a range everywhere from where reaction dominates over diffusion to systems where diffusion dominates over reaction exists.

In this study we will primarily focus on higher Pe number cases in the range $Pe \geq 100$ since these are known to be more difficult to upscale and because these can be thought of as cases where the asymptotic timescales/lengthscales at which Taylor dispersion ideas hold are the largest. We will focus primarily on larger Damkohler numbers, $10 < Da < 10{,}000$, where reaction timescales are much faster than diffusion timescales and the system is diffusion limited. The desired range of these dimensionless parameters is obtained by setting $\bar{u} = 1$, $2\bar{h} = 1$ (in arbitrary units) and tuning D and α to obtain the correct values of Pe and Da.

2.5. Effective transport models

As discussed in Section 1, one of the goals of Taylor dispersion is to reduce the fully dimensional transport problem to a one-dimensional effective model that adequately captures longitudinal transport through the domain of interest. Our approach aims to do the same, but with the goal of developing a model that is valid at pre-asymptotic times also.

In this section we propose two upscaled models which fall under the broad family of random walk models and, in the same manner as the random walk model described above to simulate transport at the microscale, we discretize the solute plume into a large number of solute particles. Unlike the random walk described above, we do not update a particle's position using a random jump based on a fixed time step, but rather fix a spatial jump and make the amount of time it takes for a particle to travel this distance random, much like is done in certain continuous time random walk frameworks (Berkowitz et al., 2006). Thus at a given step n a particle's state is defined by its position $x_i^{(n)}$ and time $t_i^{(n)}$. These can be grouped into vectors $\mathbf{x}^{(n)}$ and $\mathbf{t}^{(n)}$, describing the state of the full particle population. The equation for transport, updating space and time of each particle, is given by

$$\begin{aligned} \mathbf{x}^{(n+1)} &= \mathbf{x}^{(n)} + \Delta\mathbf{x}^{(n)} \\ \mathbf{t}^{(n+1)} &= \mathbf{t}^{(n)} + \Delta\mathbf{t}^{(n)}. \end{aligned} \quad (8)$$

Generally Δt and Δx can both be random with joint distribution $\psi(x, t)$. In this study, as is commonly done, we consider them independent such that $\psi(x, t) = \psi(t)\phi(x)$. Additionally we assume that the spatial step is fixed, that is $\phi(x) = \delta(x - \Delta x)$ or in any step all particles jump an equal distance Δx. By fixing Δx, we assume that the statistics of the velocity field are stationary over this length scale. For a periodic system, such as the one considered here, a natural choice of Δx is L, the length of a periodic element. To date, there is little formal development on constraints on the choice of Δx and more is needed; however, in this work, since L is the smallest scale over which the statistics of the velocity field are stationary, choosing $\Delta x < L$ would likely be problematic. Now the only random component in Eq. (8) is the time step $\Delta\mathbf{t}$. $\psi(t)$, the distribution from which this time step is sampled, is given by the travel time distribution that it takes particles to traverse one 'pore'.

In certain instances it has been common to consider successive values of $\Delta\mathbf{t}$ to be independent and identically distributed, a feature that allows the use of generalized central limit theorems to demonstrate convergence to stable distributions as well as asymptotic calculations of a plume's spatial moments (Shlesinger, 1974). However, a growing body of evidence demonstrates that this assumption can be questionable in certain systems, particularly at pre-asymptotic times in large Peclet number systems (Le Borgne et al., 2012; De Anna et al., 2013; Bolster et al., 2014). Instead it has been proposed

that successive steps are not independent and that correlation effects must be included, that is that $\Delta\mathbf{t}^{(n+1)}$ should be conditioned on the value of $\Delta\mathbf{t}^{(n)}$. Physically for the system considered here, one can justify this argument as follows: if a particle sits on a fast streamline at the center of the pore, it will traverse that pore quickly; in the absence of strong diffusion, which is what enables particles to hop across streamlines, it is likely that the particle will continue to sit on the same or similarly fast streamline (near the center) as it traverses the next pore. Likewise a particle that sits on a slow streamline near the reactive region and travels slowly through the first pore is most likely to traverse the following pore on a similarly slow streamline and may even get swept up in a nearby recirculation zone for some time. Thus successive steps must reflect this correlation. In the case of zero diffusion, perfect correlation will exist (i.e. successive jumps will be identical) and as diffusion becomes stronger this correlation lessens. In terms of the dimensionless numbers characterizing this system, the larger the Peclet number, the larger this correlation effect is going to be. For a detailed discussion on this see Bolster et al. (2014). In this study we will implement the model described in Eq. (8) in two forms: (i) a model that does not incorporate correlation between successive steps, called the uncorrelated model and (ii) a model that enforces correlation between successive time steps, called the Spatial Markov or correlated model.

The model as described so far does not explicitly incorporate chemical reactions. In addition to the random amount of time it takes a particle to cross distance $\Delta x^{(n)}$ there is a probability $\hat{P}$ that it will react during that transition. $\hat{P}$ is distinct from the probability P in the random walk model described above (it depends on the total amount of time a particle spends in the reactive layer during a transition). Since when a reaction occurs a particle disappears from the system, one possible (numerically) practical implementation is to say that a particle that reacts within the space step $\Delta x^{(n)}$ takes an infinitely long time to travel over the next and all following space steps ($\Delta x^{(n+1)}$, $\Delta x^{(n+2)}$, …). Thus we can naturally incorporate the occurrence of reactions into the transition time distribution by saying that it is the distribution of times it takes for all particles that make it across the transition ($\psi_a(t)$) plus a delta pulse located at infinity, appropriately weighted to account for the number of particles that react during a given transition ($\psi_\lambda(t) = M\delta(t-\infty)$ where M is the proportion of particles that have reacted out of the system within that step). In this case $\Delta t = \infty$ may be considered to be a limbo state (Van Kampen, 1992). Any particle with the temporal state $\Delta t = \infty$ means that it is no longer in the spatial domain and no longer participates in the random walk process (i.e. it has reacted out of the system). Thus $\psi(t) = \psi_a(t) + \psi_\lambda(t)$ such that $\int_T \psi(t)dt = 1$ where the subscript T denotes integration over the interval $[0, +\infty]$ of the extended real line.

For the uncorrelated model the only ingredient required is the transition time distribution (defined with the limbo state as described above). However, for the Spatial Markov model we need the transition time distribution, as well as a manner of imposing the correlation between successive time steps and the likelihood of reaction. Successive correlation is imposed via the transition matrix, described below.

2.6. Inputs for the uncorrelated and Spatial Markov models

Here we define the inputs that must be obtained from the microscale domain in order to build the macroscale effective Spatial Markov model. In all cases in order to obtain these metrics we run the random walk model described in Section 2.3 with a pulse initial condition at the throat of a pore, (see Fig. 1) and simulate advection–diffusion-reaction across two periodic unit cells. The periodic unit cell corresponds to the blown up region in Fig. 1.

2.6.1. Unit cell first passage times

The first key ingredient for the Spatial Markov model is the distribution of travel times $\psi(\Delta t)$, which for the system here is the distribution of times it takes particles to travel across a unit cell or $\Delta x = L$. This is obtained by measuring the first passage time for particles to cross the first unit cell in our microscale simulations described in Section 2.3. That is, we measure the amount of time it takes each particle to first reach a distance $x = L$ and from this build the distribution $\psi(\Delta t)$. Note that particles that do not survive the transition across $\Delta x = L$, due to the reaction, are assigned to the limbo state. M, the size of the limbo state described in Section 2.5, is measured as the fraction of particles that do not survive the transition. $\hat{P}$, the probability that a particle does not survive the transition, is given by M for the uncorrelated model. For the Spatial Markov model, it is different and discussed below.

2.6.2. Transition matrix

The second key ingredient to the Spatial Markov model is accounting for correlation between successive steps, which requires us to define the conditional probability density $r(\Delta t|\Delta t')$, which characterizes the probability of having a time increment Δt given that the previous time step was $\Delta t'$. If correlation were non-existent in the system, the conditional probability would be independent of $\Delta t'$ and the conditional distribution would equal the distribution of travel times: $r(\Delta t|\Delta t') = \psi(\Delta t)$. When correlation is important this is not true. Quantifying this correlation formally is challenging and so we adopt the discrete 'transition matrix' approach introduced by Le Borgne et al. (2008a).

We begin by discretizing $\psi_a(\Delta t)$ into a finite number n of discrete classes in the range C_i ($1 \le i \le n$); a particle resides in previous step bin C_i if the transition time associated with its last step lies in the range $\Delta t_i \le \Delta t' < \Delta t_{i+1}$. The discretization is performed such that each class is equiprobable, that is an equal number of particles reside in each bin (or said otherwise occupies an equal area under the travel time distribution). We chose this method as it has been shown to work reliably for this geometry in previous studies on conservative transport (Le Borgne et al., 2011), although alternative discretizations distributing particle numbers logarithmically are also possible, if for example it is desirable to resolve tailing features in a more detailed manner. To determine the next time step we can choose from $n+1$ bins, which correspond to the same n bins from the discretization of $\psi_a(\Delta t)$ as well as one additional bin, which indicates that a particle has reacted. Thus, in the Spatial Markov model $\hat{P}_i$, the probability of reaction during a step is a vector quantity representing the probability a particle does not survive the transition given that it began in class i. Thus the transition matrix is of size $n \times (n+1)$. Now given these classes

we can discretize $r(\Delta t|\Delta t')$ into a transition probability matrix that provides the probability of jumping between classes between successive time steps. The transition matrix is defined as

$$T_{ij} = \frac{\int_{\Delta t_i}^{\Delta t_{i+1}} \int_{\Delta t_j}^{\Delta t_{j+1}} r(t|t')\psi(t')\, dt'\, dt.}{\int_{\Delta t_i}^{\Delta t_{i+1}} \psi(t')dt'} \quad (9)$$

T_{ij} represents the probability that a particle will jump from class i to class j between successive steps. T_{ij} is calculated numerically by tracking the amount of time it takes a particle to cross the first pore, assigning its class and then tracking how long it takes that same particle to cross the second pore (or react) and assigning that class. In the implementation of the Spatial Markov model a random number sampled from a uniform distribution is used in combination with the transition matrix to determine which new class a particle jumps to, from which its next transition time is sampled. How to choose an appropriate number of bins to discretize the transition matrix is still a formally open question, but in Le Borgne et al. (2012) it was shown that reliable effective models can be built with as few as 10 classes. In this study we use 50 bins, which was found to provide virtually identical results to 25 bins, suggesting convergence. We also ran the model with 100 bins, again with no appreciable changes.

It should be noted that while the transition matrix here is created using and then applied to one particular initial condition, in principle, the transition matrix encodes information valid for other initial conditions. To solve for a different initial condition, one would have to identify which class particles associated with the initial condition belong to and then march them through space and time in the same manner as described above. Another nice feature of the transition matrix is that it can be used to predict the length scales over which correlation effects are important in the system (we refer to Bolster et al. (2014) for a detailed discussion on this).

2.7. Observables to test model

The main observable that we use to validate the performance of the Spatial Markov model as an upscaled model is its ability to predict downstream BTCs at multiple distances of $x = 5L$, 10 L, 25 L and 50 L. Multiple downstream points are chosen because it is often possible to match one downstream point well given model flexibility, but it is expected that only a physically consistent model would match well at all these locations. Thus high resolution simulations, which resolve the complete motion and reaction of particles at the microscale, using Eqs. (4) and (6), are run for all conditions, the results of which are taken as the ground truth against which the upscaled model is tested.

3. Results

3.1. Travel time distributions

The travel time distributions for all considered cases are depicted in Fig. 2. The figure consists of two parts. The top row depicts $\psi_a(t)$, the travel time distribution associated with all particles that make it through without reacting. The bottom row depicts the strengths of the additional limbo space $\psi_\lambda(t) = M\delta(t - \infty)$, which corresponds to the fraction of particles that react as they pass through the first pore.

Focusing first on the distributions $\psi_a(t)$ we note that for both Peclet numbers the early arrival times up to the peak of the distribution are essentially the same for all of the considered Damkohler numbers. This is unsurprising, because this corresponds to the fastest moving particles in the system, which are those at the center of the channel, furthest away from the reactive region and thus with very small, if any, probability of reacting. Thus we expect them to behave the same regardless of how fast the reaction, or alternatively how large the Damkohler number, is.

However, the later times in the distributions clearly reflect the influence of the Damkohler number. As the Damkohler number increases (i.e. the relative influence of reaction rates becomes more important) more and more mass is lost from the tail due to reactions with the cutoff in the distribution happening earlier for larger values of Da. This is exactly reflected in the bottom part of the figure where the strength of the limbo states M systematically increase with Damkohler number and account for the amount of mass lost during the transition. We also note that for a given value of Da increasing Pe leads to a decrease in this strength, reflecting the fact that when diffusive effects are less important compared to advective effects, less mass enters the reactive region and so a greater number of particles can make it through the transition without jumping into limbo.

3.2. Transition matrices

The transition matrices for all of the considered cases are shown in Fig. 3. Note that the probabilities in the matrices are plotted logarithmically ($\log_{10}\ T_{ij}$) to highlight differences more clearly. The vertical axis of the transition matrices corresponds to bins in the previous step and the horizontal axis to the bin of the next step. Bin 1 corresponds to the fastest moving particles and bin 50 to the slowest moving ones.

To those familiar with such matrices the largest part of them displays a structure commonly observed in most studies to date, particularly for the $Pe = 1000$ case. They are diagonally banded matrices with the highest values along the primary diagonal, which physically reflects the fact that a particle's most likely transition time is close to its previous one. For the $Pe = 100$ case this is much less apparent and only subtly detectable, which reflects the fact that for smaller Peclet number correlation effects are much smaller and particles can jump between bins more freely. Similar observations were made by Bolster et al. (2014), who demonstrated that for conservative transport correlation effects are only important for $Pe > O(100)$.

Unlike in previous studies, though, there is an additional column in the transition matrices, the rightmost column, corresponding to the probability that a particle will react in its current step given its previous time step (alternatively said – enter the limbo state), which displays some telling and interesting features. Given that it is difficult to see the details of this additional column in the current format of the transition matrices, a plot showing only this column is provided in Fig. 4. For the $Pe = 100$ and $Da = 1000$ and 10,000 cases, regardless of

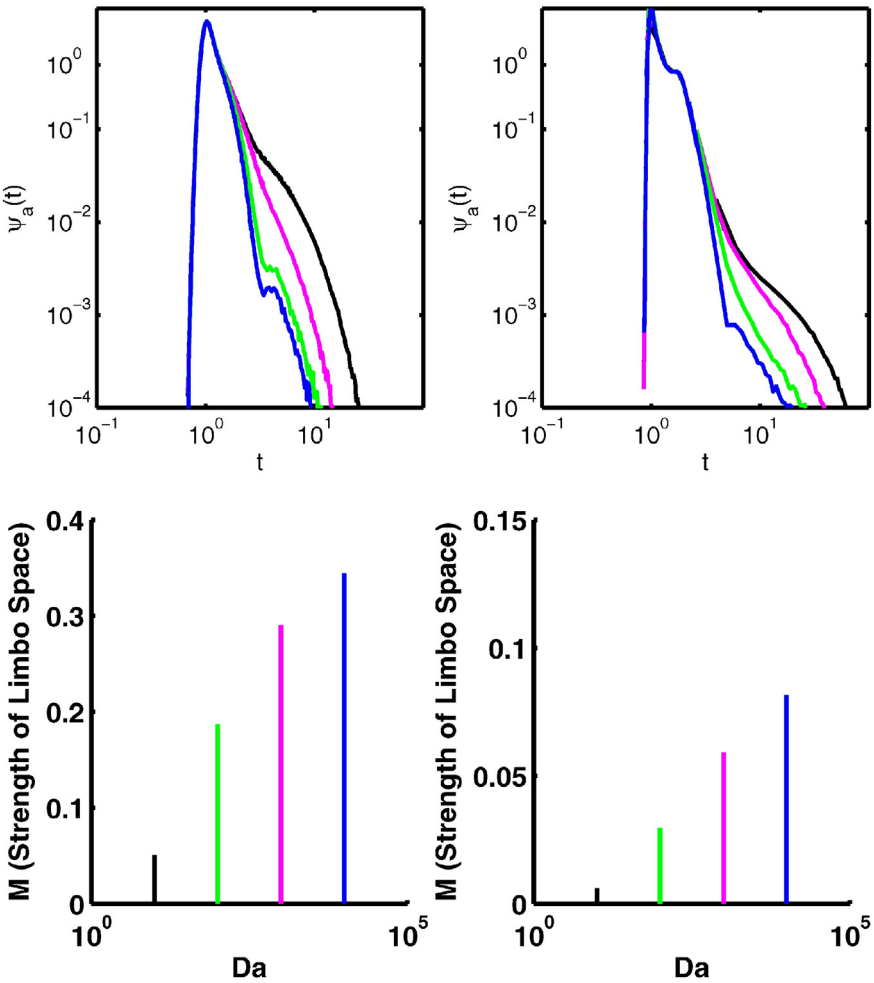

Fig. 2. Transition time distributions for $Pe = 100$ (left) and $Pe = 1000$ (right) for $Da = 10$ (black), $Da = 100$ (green). $Da = 1000$ (magenta) and $Da = 10000$ (blue). Recall that $\psi(t) = \psi_a(t) + M\delta(t - \infty)$. The top row of the figure shows $\psi_a(t)$, the travel time distribution for particles that make it through the pore and the bottom row shows the strength of the delta function corresponding the limbo state, M (i.e. representing particles that react and leave the system). (For interpretation of the references to color in this figure legend, the reader is referred to the web version of this article.)

a particle's previous time step, it has quite a high probability of reacting during its next step. This is reflected as strong red bands in the transition matrices in Fig. 3 and as relatively flat high probabilities in Fig. 4. Two features are noteworthy in Fig. 4. First, as Damkohler number decreases we see that the probability of reaction decreases across all bins (i.e. lower Damkohler number means that a particle needs to spend more time in the reactive zone to actually react); second the higher number bins (slowest moving particles) have greater probability of reaction than the lower bins (faster particles). The nonuniform nature of this probability suggests that correlation effects may be important even for the smaller Peclet number, in a way that they may not be for conservative transport.

This feature is even more apparent in all of the $Pe = 1000$ cases, along with the fact that the probability of reaction for the fastest moving particles is pretty much zero. This reflects that due to the larger Peclet number (smaller relative diffusive effects) the probability of entering the reactive zone, which can only be achieved by diffusion, is almost zero, thus precluding the possibility of a reaction occurring. Thus only particles that traveled slowly across the previous transition have a realistic probability of reaction in the next one.

3.3. BTCs — a comparison of high resolution microscale simulations and the effective upscaled models

Results of the BTCs measured from the micro-scale simulations and as predicted by uncorrelated and Spatial Markov model are presented in Figs. 5–8. One of the major aspects to note in these BTCs is the influence of reaction in the system. Much as in the unit cell transition time distributions, as the Damkohler number increases (reaction becomes stronger) less and less mass makes it to each downstream position, with later time arrivals in particular being cut off the most as these are the slowest particles that are most likely to have passed through the slow reactive regions in our system. In fact for the $Pe = 100$ case in all but the $Da = 10$ case, virtually none of the solute makes it to the $x = 50L$ measurement point as diffusive and reactive effects are strong enough to ensure that solute moves through the reactive zone for sufficient time for the

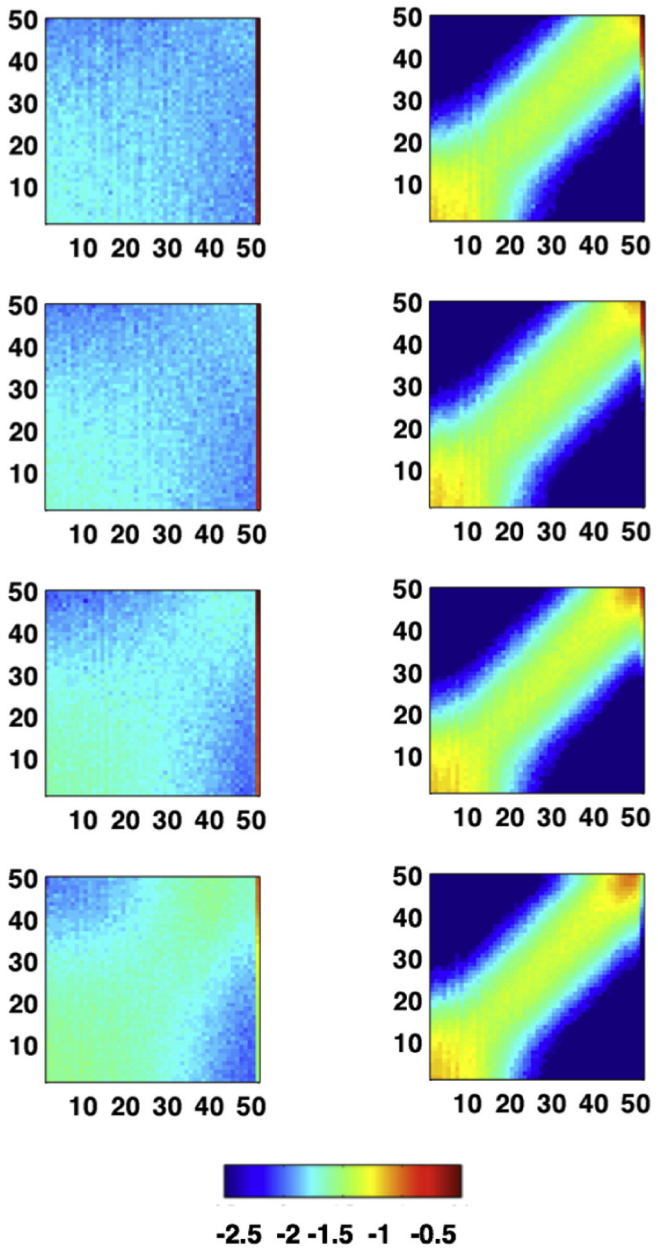

Fig. 3. Transition matrices ($\log_{10} T_{ij}$) for $Pe = 100$ (left) and $Pe = 1000$ (right), and for $Da = 10000$ (top row), $Da = 1000$ (2nd row), $Da = 100$ (3rd row), and $Da = 10$ (bottom row). The rows of the transition matrices correspond to the previous step and the columns correspond to the current step.

solute to be removed. These are essential features that the upscaled models must be able to capture.

In all cases, spanning the full range of considered Damkohler and Peclet numbers, the agreement between prediction and observations for the Spatial Markov model is excellent (Figs. 6 and 8), suggesting that it is able to successfully predict the evolution of the tracer under the reactive conditions considered in this system.

On the other hand, the uncorrelated model (Figs. 5 and 7) captures some of the essential features, but behaves less favorably than the Spatial Markov model. Mismatches between the model and measurements are worse for the higher *Pe* number case, which is in line with our intuition that larger Peclet numbers mean greater need to incorporate correlation. Nonetheless, even for the $Pe = 100$ cases, the uncorrelated model does not accurately capture the early arrival of the breakthrough curves with a delay in the peak for the $x = 5$ and 10 L cases and a shift in the further downstream breakthrough curves (for the $Da = 10$ case). The underprediction of early arrival concentrations is systematic across all Damkohler numbers. This reflects the fact that the model does not enforce correlations among fast moving particles correctly which allows particles to react out of the system that should not do so. For the greatest downstream distance the model has

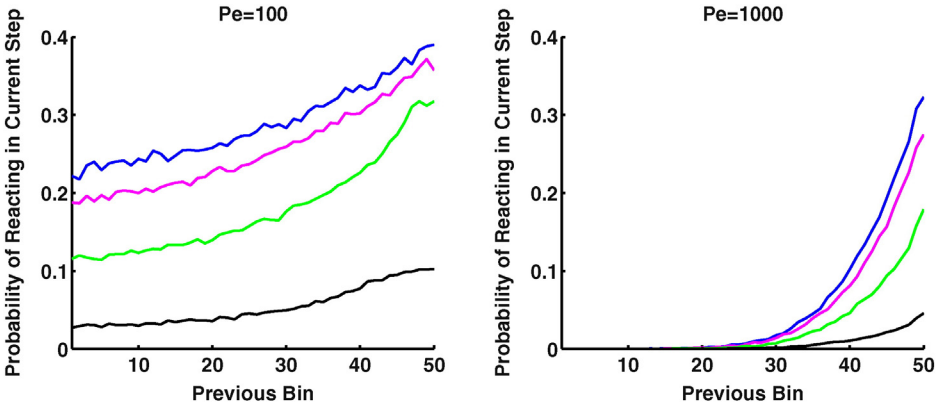

Fig. 4. The rightmost column of the transition matrices for $Pe = 100$ (left) and $Pe = 1000$ (right) and $Da = 10$ (black), $Da = 100$ (green), $Da = 1000$ (magenta) and $Da = 10000$ (blue). These curves represent the probability of a particle reacting out of the system in the current step given the transition time bin in the previous step. (For interpretation of the references to color in this figure legend, the reader is referred to the web version of this article.)

allowed most of the mass to react out of the system for all $Da \geq 100$ cases, but the results from the upstream breakthrough curves and the mismatches of early arrivals, suggest that it may have reacted out of the system too quickly. These issues are even more evident in the $Pe = 1000$ cases where early arrivals and a truncation of the tail concentrations occur throughout.

The above results are consistent with knowledge from previous studies on conservative transport, that is that correlation effects are more pronounced and therefore must be incorporated into an upscaled model as Peclet numbers become larger, or better said as diffusive effects become weaker relative to advective ones. However, the results also suggest that the critical Peclet number to adequately capture reactive effects may be smaller than one estimated for the conservative case. Bolster et al. (2014) showed for a very similar geometry that correlation effects were negligible for $Pe = 100$, while for the reactive case they appear to play a more significant role.

3.4. Total mass in breakthrough curves

A characteristic in the case of reactive transport is that not all of the mass injected makes it to each of the downstream locations. Thus another useful measure of a model's success is how well it reproduces the total amount of mass in each breakthrough curve. Fig. 9 depicts this for both Peclet and all Damkohler numbers. This metric is particularly useful in highlighting mismatches between the models and observations, which may be obfuscated in the detailed breakthrough curves. In all cases we see that the correlated or Spatial Markov model does an excellent job of matching the observations with a maximum error of 5% (which is the absolute worst case – most are less than 0.1%), while the uncorrelated model has errors as large as 91%, underpredicting the total mass by as much as an order of magnitude.

In all cases there appears to be an exponential decay of mass with downstream distance, suggesting use of an effective first order rate with distance would be reasonable. This effective rate systematically increases with increasing *Da*, in line with the fact that as *Da* increases the amount of reaction increases also. However, neglecting correlation overpredicts this effective reaction rate and the overprediction becomes worse as *Da* increases, suggesting that the higher the *Da* the more important it is to include correlation. Indeed, while there are some mismatches in early arrivals of the breakthrough curves for the lowest *Da* cases, the uncorrelated model fairly accurately predicts the total mass arriving, although the maximum error is still of order 10%, which is worse than the correlated model. Likewise as the *Pe* number increases the prediction gets worse, much like observations from conservative transport studies. Thus when considering the importance of correlation effects in an upscaled model it is important to consider diffusive effects relative to both advective and reactive effects, as quantified by a *Pe* and *Da* number.

4. Conclusions

We have investigated reactive transport in an idealized flow, that is a periodic channel with a sinusoidal boundary, where reactions are confined to a diffusive layer of finite extent adjacent to the flow channel. Specifically, we have tested the ability of two upscaled random walk models to effectively reproduce breakthrough curve observations from fully resolved simulations that explicitly resolve the full flow, diffusion, and reaction dynamics across a range of Peclet and Damkohler number conditions. Both random walk models aim to describe effective transport by discretizing solute into a large number of particles that make successive jumps of finite size, the length of a periodic element, but with random times, sampled from a measured transition time distribution. One of the models, the uncorrelated model, assumes that the time steps between successive jumps are independent and identically distributed, while the second model, the Spatial Markov model, enforces correlations between successive transition times, also measured from the fully resolved simulations.

We demonstrate that the Spatial Markov model is able to reasonably reproduce the structure and amount of mass in each of the breakthrough curves measured from the fully resolved simulation across the range of considered Peclet and Damkohler numbers, which were chosen as being physically representative, as well as in the range where upscaling might be most challenging. On the other hand, the uncorrelated model provides less accurate predictions, which become worse

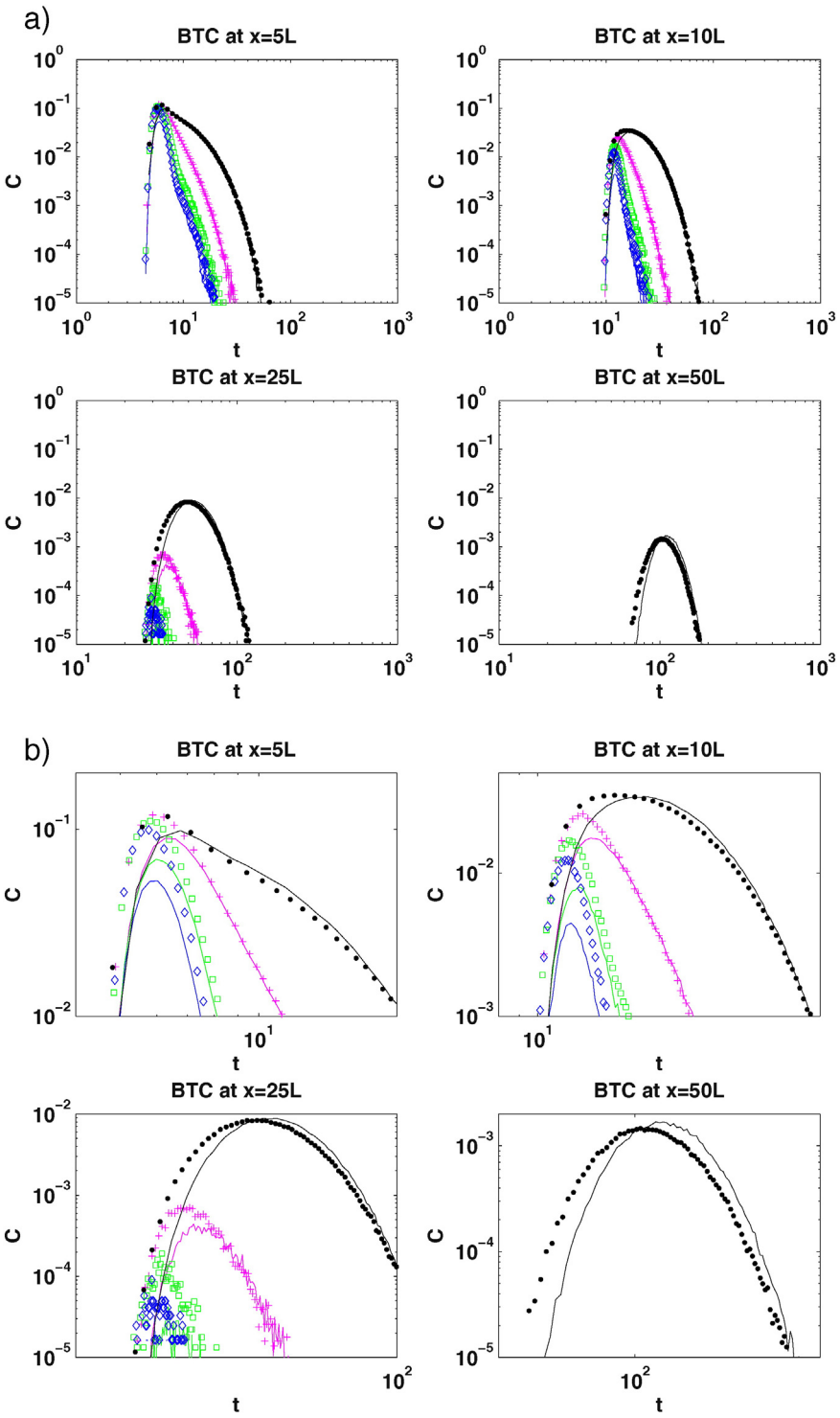

Fig. 5. Breakthrough curves for $Pe = 100$ and $Da = 10$ (black dots), $Da = 100$ (magenta plus), $Da = 1000$ (green squares) and $Da = 10000$ (blue diamonds). Solid lines correspond to predictions with the uncorrelated model while symbols correspond to observations from the fully resolved microscale simulations. The upper four panels show the full BTCs, while the lower panels highlight the early arrivals to demonstrate the most significant mismatches. (For interpretation of the references to color in this figure legend, the reader is referred to the web version of this article.)

as Peclet and Damkohler numbers increase. While it is well known from previous studies that an increase in Peclet number will require the enforcement of successive correlations to ensure better predictions, a previous study (Bolster et al., 2014) shows that for a very similar setup to the one considered here, these effects only become important when

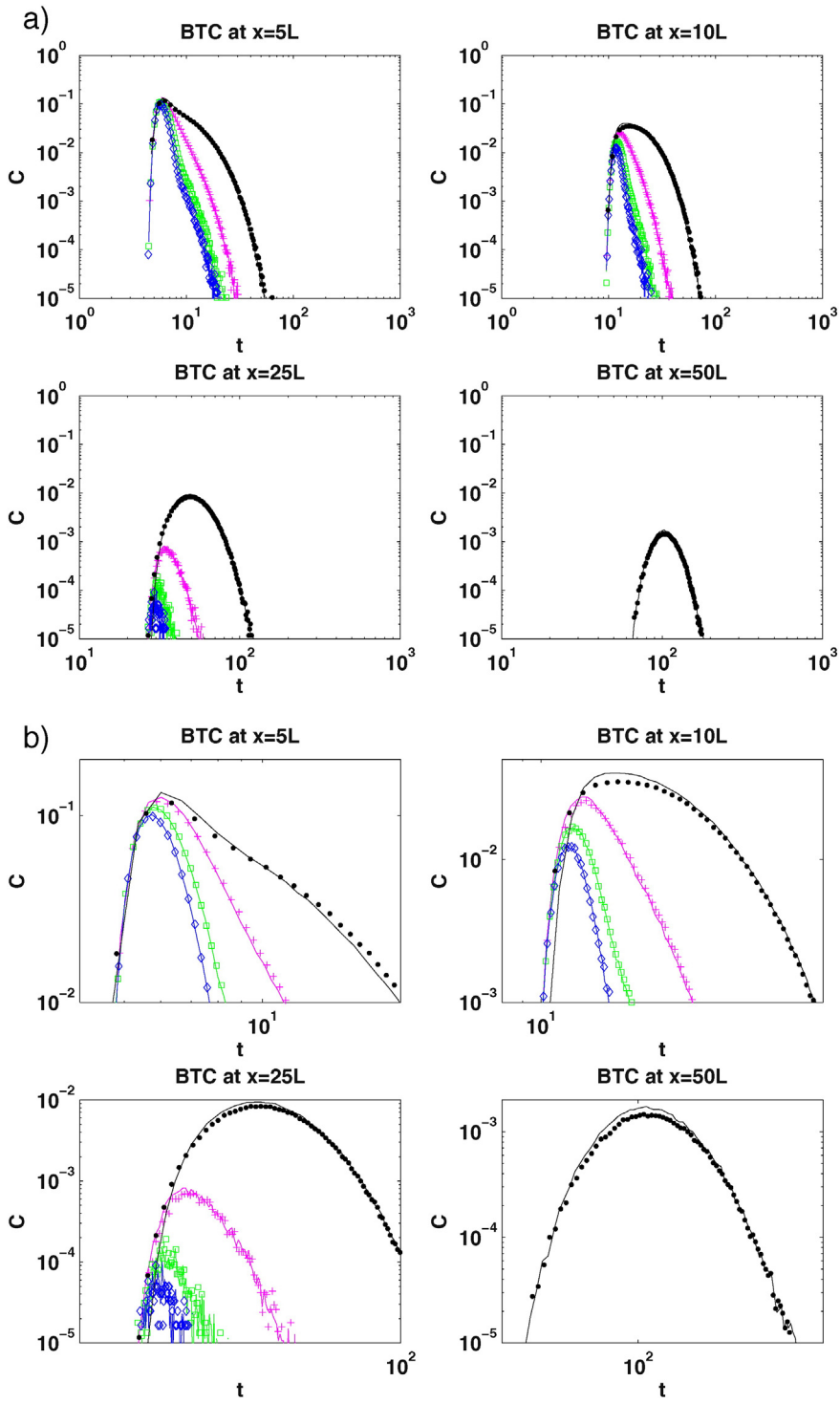

Fig. 6. Breakthrough curves for $Pe = 100$ and $Da = 10$ (black dots), $Da = 100$ (magenta plus), $Da = 1000$ (green squares) and $Da = 10000$ (blue diamonds). Solid lines correspond to predictions with the Spatial Markov model while symbols correspond to observations from the fully resolved microscale simulations. The upper four panels show the full BTCs, while the lower panels highlight the early arrivals. (For interpretation of the references to color in this figure legend, the reader is referred to the web version of this article.)

$Pe > O(100)$ for the case of a conservative tracer. In the presence of reactions, such as is considered here, this restriction appears to be greater and the importance of imposing correlations in successive jumps is critical to reproducing many pertinent features observed in the small scale fully resolved simulations.

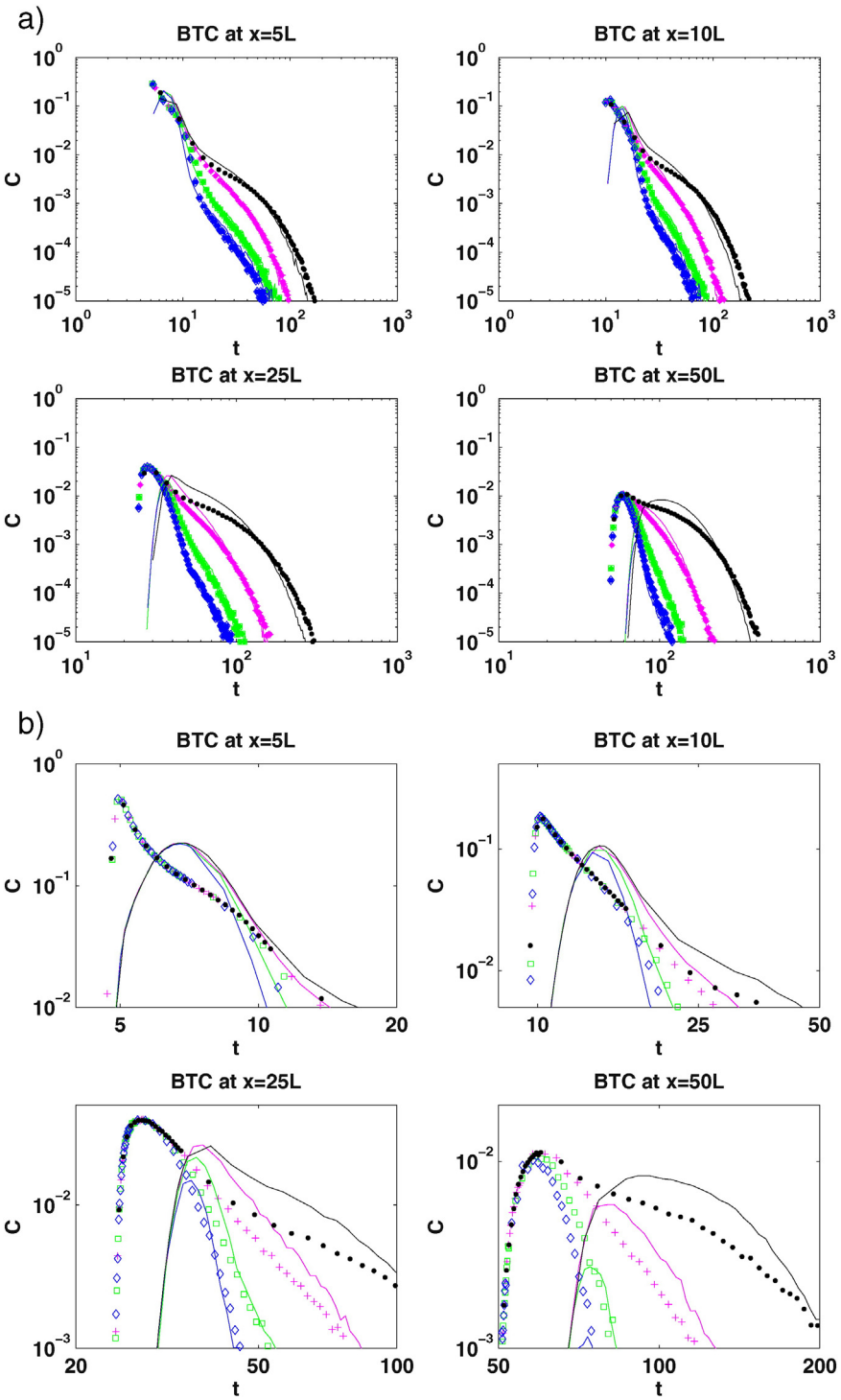

Fig. 7. Breakthrough curves for $Pe = 1000$ and $Da = 10$ (black dots), $Da = 100$ (magenta plus), $Da = 1000$ (green square) and $Da = 10000$ (blue diamond). Solid lines correspond to predictions with the uncorrelated model while symbols correspond to observations from the fully resolved microscale simulations. The upper four panels show the full BTCs, while the lower panels highlight the early arrivals to demonstrate the most significant mismatches. (For interpretation of the references to color in this figure legend, the reader is referred to the web version of this article.)

While the geometry considered here is incredibly simple, it and very similar geometries have proven to be valuable case studies to understand, interpret and model transport in porous/fractured media. As such, while this study by no means definitely demonstrates the ability of the Spatial Markov model to upscale reactive transport in the context of a

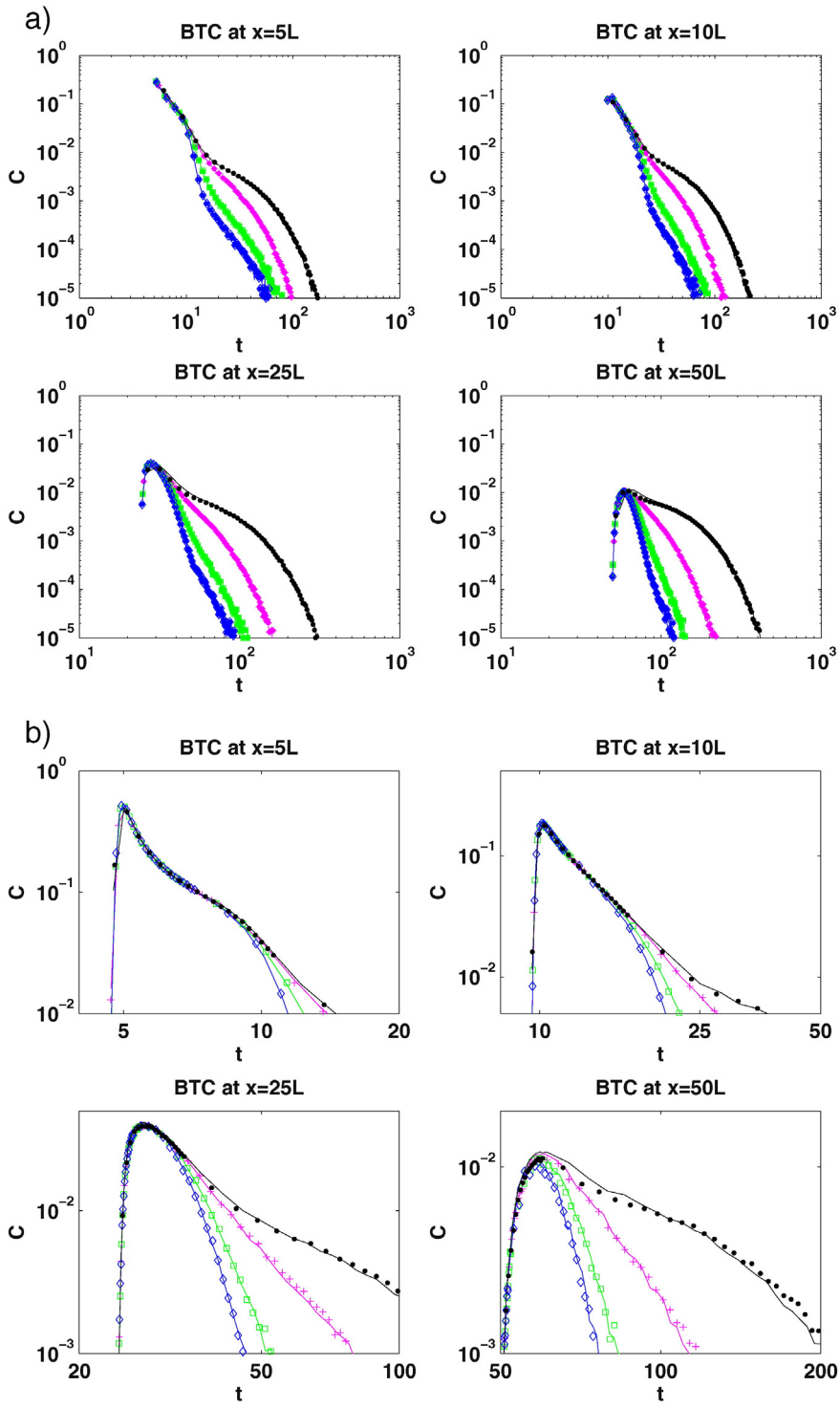

Fig. 8. Breakthrough curves for $Pe = 1000$ and $Da = 10$ (black dots), $Da = 100$ (magenta plus), $Da = 1000$ (green square) and $Da = 10000$ (blue diamond). Solid lines correspond to predictions with the Spatial Markov model while symbols correspond to observations from the fully resolved microscale simulations. The upper four panels show the full BTCs, while the lower panels highlight the early arrivals. (For interpretation of the references to color in this figure legend, the reader is referred to the web version of this article.)

heterogeneously distributed degradation rate, it does demonstrate the promise that such a modeling approach holds and lays the foundation for future work to test it in more complex and realistic configurations, where for conservative transport it has already had significant successes. Additionally, it must be noted that one of the reasons the Spatial Markov model can

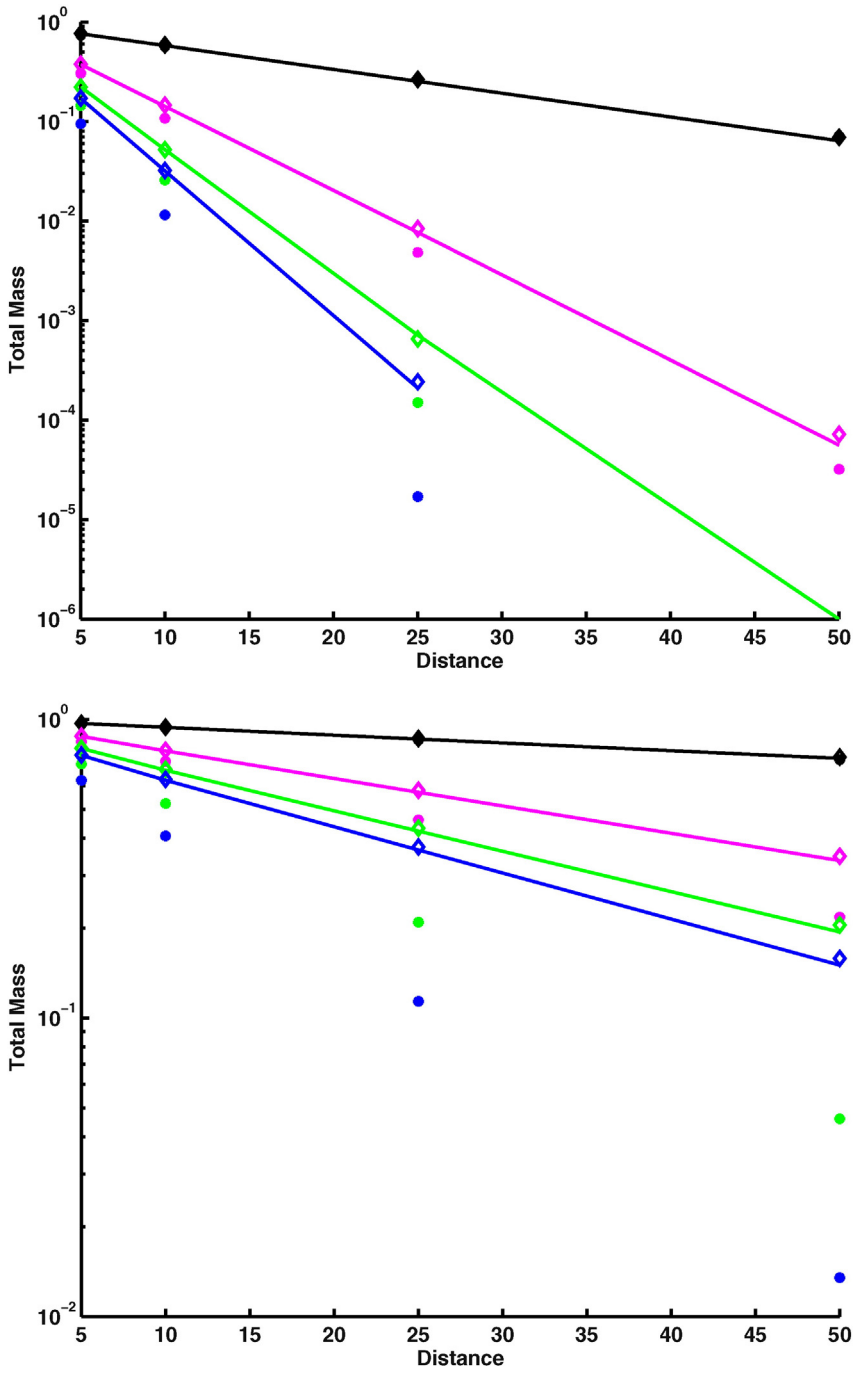

Fig. 9. Total mass in breakthrough curves at distances $x = 5L$, 10 L, 25 L and 50 L for $Pe = 100$ (top) and $Pe = 1000$ (bottom) and $Da = 10$ (black), 100 (magenta), 1000 (green) and 10,000 (blue). Measured mass from the high resolution microscale simulations are depicted with the solid lines, Spatial Markov predictions with ◇, and the uncorrelated model predictions with •. (For interpretation of the references to color in this figure legend, the reader is referred to the web version of this article.)

readily be generalized to incorporate the simple type of reaction considered here is that the reaction rate is linear with concentration. While reasonable in certain instances, many reactions of interest are nonlinear and the methods proposed here cannot be applied without some further effort and modification. However, by merging the ideas presented here with recent advances in Lagrangian reactive particle methods (e.g. Benson and Meerschaert, 2008; Ding et al., 2013; Paster et al., 2013; Paster et al., 2014), it may be possible to generalize reactive Spatial Markov methods even further.

Acknowledgments

We would like to express thanks for the financial support via the Army Office of Research grant W911NF1310082 and NSF grants EAR-1351623 and EAR-1417264.

References

Aris, R., 1956. On the dispersion of solute in a fluid flowing through a tube. Proc. R. Soc. Lond. Ser. A 235, 67–77.
Battiato, I., Tartakovsky, D., 2011. Applicability regimes for macroscopic models of reactive transport in porous media. J. Contam. Hydrol. 120, 18–26.
Battiato, I., Tartakovsky, D.M., Tartakovsky, A.M., Scheibe, T., 2009. On breakdown of macroscopic models of mixing-controlled heterogeneous reactions in porous media. Adv. Water Resour. 32 (11), 1664–1673.
Benson, D.A., Meerschaert, M.M., 2008. Simulation of chemical reaction via particle tracking: Diffusion-limited versus thermodynamic rate-limited regimes. Water Resour. Res. 44, W12201. http://dx.doi.org/10.1029/2008WR007111.
Berkowitz, B., Cortis, A., Dentz, M., Scher, H., 2006. Modeling non-Fickian transport in geological formations as a continuous time random walk. Rev. Geophys. 44, RG2003. http://dx.doi.org/10.1029/2005RG000178.
Bolster, D., Borgne, T.L., Dentz, M., 2009. Solute dispersion in channels with periodically varying apertures. Phys. Fluids 21, 056601.
Bolster, D., Méheust, Y., Le Borgne, T., Bouquain, J., Davy, P., 2014. Modeling preasymptotic transport in flows with significant inertial and trapping effects—the importance of velocity correlations and a spatial Markov model. Adv. Water Resour. 70, 89–103.
Bouquain, J., Meheust, Y., Bolster, D., Davy, P., 2012. The impact of inertial effects on solute dispersion in a channel with periodically varying aperture. Phys. Fluids 24, 083602.
Brenner, H., 1980. Dispersion resulting from flow through spatially periodic porous media. Philos. Trans. R. Soc. Lond. Ser. A 297, 81–133.
Cao, J., Kitanidis, P., 1998. Adaptive finite element simulation of stokes flow in porous media. Adv. Water Resour. 22 (1), 17–31.
Cardenas, M.B., 2008. Three-dimensional vortices in single pores and their effects on transport. Geophys. Res. Lett. 35, L18402. http://dx.doi.org/10.1029/2008GL035343.
Cardenas, M.B., 2009. Direct simulation of pore level Fickian dispersion scale for transport through dense cubic packed spheres with vortices. Geochem. Geophys. Geosyst. 10, Q12014.
Chaudhary, K., Cardenas, M.B., Deng, W., Bennett, P.C., 2011. The role of eddies inside pores in the transition from Darcy to Forchheimer flows. Geophys. Res. Lett. 38. http://dx.doi.org/10.1029/2011GL050214.
Chaudhary, K., Cardenas, M., Deng, W., Bennett, P., 2013. Pore geometry effects on intrapore viscous to inertial flows and on effective hydraulic parameters. Water Resour. Res. 49, 1149–1162.
De Anna, P., Le Borgne, T., Dentz, M., Tartakovsky, A.M., Bolster, D., Davy, P., 2013. Flow intermittency, dispersion, and correlated continuous time random walks in porous media. Phys. Rev. Lett. 110 (18), 184502.
Dentz, M., Le Borgne, T., Englert, A., Bijeljic, B., 2011. Mixing, spreading and reaction in heterogeneous media: a brief review. J. Contam. Hydrol. 120, 1–17.
Ding, D., Benson, D.A., Paster, A., Bolster, D., 2013. Modeling bimolecular reactions and transport in porous media via particle tracking. Adv. Water Resour. 53, 56–65.
Dykaar, B., Kitanidis, P., 1996. Macrotransport of a biologically reacting solute through porous media. Water Resour. Res. 32, 307–329.
Gillis, J., 1955. Correlated random walk. Mathematical Proceedings of the Cambridge Philosophical Society vol. 51. Cambridge Univ Press.
Goldstein, S., 1951. On diffusion by discontinuous movements, and on the telegraph equation. Q. J. Mech. Appl. Math. 4 (2), 129–156.
Haus, J.W., Kehr, K.W., 1987. Diffusion in regular and disordered lattices. Phys. Rep. 150 (5), 263–406.
Hornung, U., 1997. Homogenization and Porous Media. Springer.
Kang, P.K., Dentz, M., Le Borgne, T., Juanes, R., 2011. Spatial Markov model of anomalous transport through random lattice networks. Phys. Rev. Lett. 107 (18), 180602.
Kang, P.K., Anna, P., Nunes, J.P., Bijeljic, B., Blunt, M.J., Juanes, R., 2014. Pore-scale intermittent velocity structure underpinning anomalous transport through 3-d porous media. Geophys. Res. Lett. 41 (17), 6184–6190.
Kang, P.K., Le Borgne, T., Dentz, M., Bour, O., Juanes, R., 2015. Impact of velocity correlation and distribution on transport in fractured media: Field evidence and theoretical model. Water Resour. Res 51, 940–959. http://dx.doi.org/10.1002/2014WR015799.
Kinzelbach, W., 1988. The random walk method in pollutant transport simulation. Groundwater Flow and Quality Modelling. Springer, pp. 227–245.
Kitanidis, P., Dykaar, B., 1997. Stokes flow in a slowly varying two-dimensional periodic pore. Transp. Porous Media 26, 89–98.
Le Borgne, T., Dentz, M., Carrera, J., 2008a. Lagrangian statistical model for transport in highly heterogeneous velocity fields. Phys. Rev. Lett. 101, 090601.
Le Borgne, T., Dentz, M., Carrera, J., 2008b. Spatial Markov processes for modeling Lagrangian particle dynamics in heterogeneous porous media. Phys. Rev. E 78, 026308.
Le Borgne, T., Bolster, D., Dentz, M., de Anna, P., Tartakovsky, A., 2011. Effective pore-scale dispersion upscaling with a correlated continuous time random walk approach. Water Resour. Res. 47, W12538. http://dx.doi.org/10.1029/2011WR010457.
Le Borgne, T., Bolster, D., Dentz, M., de Anna, P., Tartakovsky, A., 2012. Effective pore-scale dispersion upscaling with a correlated CTRW approach. Water Resour. Res. 47, W12538.
Lunati, I., Attinger, S., Kinzelbach, W., 2002. Macrodispersivity for transport in arbitrary nonuniform flow fields: asymptotic and preasymptotic results. Water Resour. Res. 38 (10), 1187. http://dx.doi.org/10.1029/2001WR001203 2002.
Paster, A., Bolster, D., Benson, D., 2013. Particle tracking and the diffusion–reaction equation. Water Resour. Res. 49 (1), 1–6.
Paster, A., Bolster, D., Benson, D.A., 2014. Connecting the dots: semi-analytical and random walk numerical solutions of the diffusion–reaction equation with stochastic initial conditions. J. Comput. Phys. 263, 91–112.
Pavlostathis, S., Giraldo-Gomez, E., 1991. Kinetics of anaerobic treatment: a critical review. Crit. Rev. Environ. Sci. Technol. 21 (5–6), 411–490.
Plumb, O., Whitaker, S., 1988. Dispersion in heterogeneous porous media: 1. local volume averaging and large-scale averaging. Water Resour. Res. 24, 913–926.
Richmond, M.C., Perkins, W.A., Scheibe, T.D., Lambert, A., Wood, B.D., 2013. Flow and axial dispersion in a sinusoidal-walled tube: Effects of inertial and unsteady flows. Adv. Water Resour 62, 215–226.
Risken, H., 1984. Fokker-Planck Equation. Springer.
Semprini, L., McCarty, P.L., 1992. Comparison between model simulations and field results for in-situ biorestoration of chlorinated aliphatics: Part 2. Cometabolic transformations. Groundwater 30 (1), 37–44.
Shapiro, M., Brenner, H., 1988. Dispersion of a chemically reactive solute in a spatially periodic model of a porous medium. Chem. Eng. Sci. 43 (3), 551–571.
Shlesinger, M., 1974. Asymptotic solutions of continuous-time random walks. J. Stat. Phys. 10, 421–433.
Sund, N., Bolster, D., Dawson, C., 2015. Pre-asymptotic transport upscaling in inertial and unsteady flows through porous media. Transp. Porous Media http://dx.doi.org/10.1007/s11242-015-0526-5 (in press).
Taylor, G.I., 1922. Diffusion by continuous movements. Proc. Lond. Math. Soc. 20 (1), 196–212.
Taylor, G., 1953. Dispersion of soluble matter in solvent flowing slowly through a tube. Proc. R. Soc. Lond. Ser. A 219, 186–203.
Van Kampen, N.G., 1992. Stochastic Processes in Physics and Chemistry vol. 1. Elsevier.
Weiss, G.H., Rubin, R.J., 1983. Random walks: theory and selected applications. Adv. Chem. Phys. 52, 363–505.
Wood, B.D., Cherblanc, F., Quintard, M., Whitaker, S., 2003. Volume averaging for determining the effective dispersion tensor: Closure using periodic unit cells and comparison with ensemble averaging. Water Resour. Res. 39, 1210. http://dx.doi.org/10.1029/2002WR001723 8.